MNRAS **000**, 000–000 (0000) Preprint 14 June 2019 Compiled using MNRAS LATEX style file v3.0

Near and Mid-infrared properties of known redshift $z \geq 5$ Quasars

Nicholas P. Ross* and Nicholas J. G. Cross
Institute for Astronomy, University of Edinburgh, Royal Observatory, Edinburgh, EH9 3HJ, United Kingdom

14 June 2019

ABSTRACT
We assemble a catalogue of 463 spectroscopically confirmed very high ($z \geq 5.00$) redshift quasars and report their near ($ZYJHK_s$ and K) infrared and mid-infrared (WISE) properties. We find that SDSS and Pan-STARRS1 together identified over half of the VHzQ sample and that 97.0% of the VHzQ sample is detected in one or more NIR ($ZYJHK/K_s$) band, with lack of coverage rather than lack of depth for the objects that are not detected in the NIR. 362 (78.2%) VHzQs are detected at 3.4μm in the W1 band from the unWISE catalog and all of the $z \geq 7$ quasars are detected in both unWISE W1 and W2. Using archival WFCAM/UKIRT and VIRCAM/VISTA data we check for photometric variability in the near-infrared that might be expected from super-Eddington accretion. We find 32 of the quasars have sufficient NIR measurements and signal-to-noise to look for variability. Weak variability was detected in multiple bands of SDSS J0959+0227, and very marginally in the Y-band of MMT J0215-0529. Two other quasars, SDSS J0349+0034 and SDSS J2220-0101 had significant differences between their WFCAM and VISTA magnitudes in one band. All the data, analysis codes and plots used and generated here can be found at: `github.com/d80b2t/VHzQ`.

Key words: Astronomical data bases: surveys – Quasars: general – galaxies: evolution – galaxies: infrared.

1 INTRODUCTION

Very high redshift quasars (VHzQ; defined here to have redshifts $z \geq 5.00$) are excellent probes of the early Universe. This includes studies of the Epoch of Reionization for hydrogen (see e.g. Fan et al. 2006a; Mortlock 2016, for reviews), the formation and build-up of supermassive black holes (e.g., Rees 1984; Wyithe & Loeb 2003; Volonteri 2010; Agarwal et al. 2016; Valiante et al. 2018; Latif et al. 2018; Wise et al. 2019) and early metal enrichment (see e.g., Simcoe et al. 2012; Chen et al. 2017; Bosman et al. 2017).

Super-critical accretion, where $\dot{M} > \dot{M}_{\rm Edd}$, is a viable mechanism to explain the high, potentially super-Eddington, luminosity and rapid growth of supermassive black holes in the early universe (e.g., Alexander & Natarajan 2014; Madau et al. 2014; Volonteri et al. 2015; Pezzulli et al. 2016; Lupi et al. 2016; Pezzulli et al. 2017; Takeo et al. 2018). Thus, one could expect VHzQs to potentially vary in luminosity as they go through phases of super-critical accretion. These signatures of photometric variability should be looked for, noting the rest-frame optical emission is redshifted into the observed near-infrared (NIR) at redshifts $z > 5$. Fortunately, data are now in place from deep, wide-field NIR instruments and surveys such as the Wide Field Camera (WFCAM) instrument on the United Kingdom Infra-Red Telescope (UKIRT) in the Northern Hemisphere and the VISTA InfraRed CAMera (VIRCAM) on the Visible and Infrared Survey Telescope for Astronomy (VISTA) in the Southern Hemisphere, that are necessary for identifying VHzQs.

Quasars are known to be prodigious emitters of infrared emission, thought to be from the thermal emission of dust grains heated by continuum emission from the accretion disc (e.g., Richards et al. 2006; Leipski et al. 2014; Hill et al. 2014; Hickox et al. 2017). Observations in the mid-infrared, e.g. ∼3-30μm allow discrimination between AGN[1] and passive galaxies due to the 1.6μm "bump" entering the MIR at $z \approx 0.8 - 0.9$ (e.g., Wright et al. 1994; Sawicki 2002; Lacy et al.

* E-mail: npross@roe.ac.uk

[1] Historically, "quasars" and "Active Galactic Nuclei (AGN)" have described different luminosity/classes of objects. In recognition of the fact that both terms describe accreting supermassive black holes, we use these terms interchangeably, with a preference for quasar, since we are generally in the higher-L regime (e.g. Haardt et al. 2016).

2004; Stern et al. 2005; Richards et al. 2006; Timlin et al. 2016) as well as between AGN and star-forming galaxies due to the presence of Polycyclic Aromatic Hydrocarbon (PAHs) at $\lambda > 3\mu$m (e.g., Yan et al. 2007; Tielens 2008).

Jiang et al. (2006) and Jiang et al. (2010) report on the discovery of a quasar without hot-dust emission in a sample of 21 $z \approx 6$ quasars. Such apparently hot-dust-free quasars have no counterparts at low redshift. Moreover, those authors demonstrate that the hot-dust abundance in the 21 quasars builds up in tandem with the growth of the central black hole. But understanding how dust first forms and appears in the central engine remains an open question (Wang et al. 2008, 2011).

WISE mapped the sky in 4 passbands, in bands centered at wavelengths of 3.4, 4.6, 12, and 23μm. The all sky 'AllWISE' catalogue release, contains nearly 750 million detections at high-significance[2], of which over 4.5M AGN candidates have been identified with 90% reliability (Assef et al. 2018). Blain et al. (2013) presented WISE mid-infrared (MIR) detections of 17 (55%) of the then known 31 quasars at $z > 6$. However, Blain et al. (2013) was compiled with the WISE 'All-Sky' data release, as opposed to the superior AllWISE catalogues. That sample only examined the 31 known $z > 6$ quasars; our sample has 170 objects with redshift $z \geq 6.00$ (with 108 detected in WISE). Bañados et al. (2016) reports WISE W1, W2, W3 and W4 magnitudes for the Panoramic Survey Telescope and Rapid Response System 1 (Pan-STARRS1, PS1; Kaiser et al. 2002, 2010), but with no further investigation into the reddest WISE waveband for the VHzQs.

Critically, we now have available to us new W1 and W2 photometry from the 'unWISE Source Catalog' (Schlafly et al. 2019), a WISE-selected catalogue that is based on significantly deeper imaging and has a more extensive modeling of crowded regions than the AllWISE release. For the first time in a catalogue, unWISE takes advantage of the ongoing mid-IR Near-Earth Object Wide-Field Infrared Survey Explorer Reactivation mission (NEOWISE-R; Mainzer et al. 2014), and achieves depths ∼0.7 mag deeper than AllWISE (in W1/2). This additional depth is a significant advantage in the detection and study of VHzQs in the 3-5 micron regime.

Here we present for the first time the combined near-infrared properties (from UKIRT and VIRCAM) and the new mid-infrared unWISE for all the spectroscopically known $z \geq 5.00$ quasars. Our motivations are numerous and include: *(i)* establishing the first complete catalogue of $z > 5.00$ quasars since the pioneering work from SDSS; *(ii)* utilizing all the WFCAM and VISTA near-infrared photometry available for the quasars; *(iii)* making the first study of near- and mid-IR variability of the VHzQ population and *(iv)* establishing the photometric properties for upcoming surveys and telescopes including the Large Synoptic Survey Telescope (LSST)[3], ESA *Euclid*[4] and the *James Webb Space Telescope* (JWST)[5,6,7,8]. We chose redshift $z = 5.00$ as our lower redshift limit due to a combination of garnishing a large sample, adequately spanning physical properties (e.g. luminosity, age of the Universe) and to highlight the parts of $L - z$ parameter space where $z > 5$ quasars still wait to be discovered.

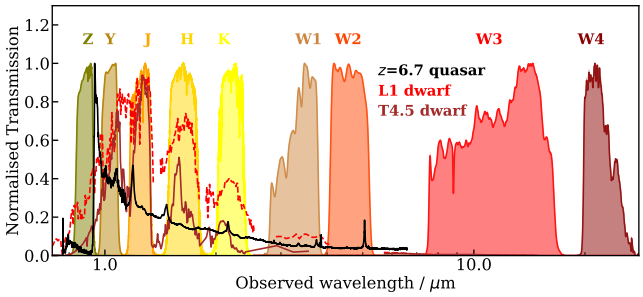

Figure 1. The spectral bands used in this paper. The $ZYJHK$ filter curves are from UKIRT/WFCAM. The $ZYJHK_s$ VISTA/VIRCAM filter curves are similar, but not identical to these. The WISE passbands W1-4 are presented, though without the Brown et al. (2014) W4 recalibration. The quasar spectrum is a composite based on Vanden Berk et al. (2001) and Bañados et al. (2016). The L and T dwarf spectra are from Cushing et al. (2006).

This paper is organized as follows. In Section 2, we present the assembled list of the 463 $z \geq 5.00$ VHzQs that we have compiled. We then give a high-level overview of the photometric surveys and datasets we use and present the photometry of the VHzQs. In Section 3 we investigate the variability properties of the VHzQs, looking for evidence of super-critical accretion. In Section 4 we calculate how many $z > 5$ quasars we should expect to find in current datasets. We conclude in Section 5 and present all the necessary details to obtain our dataset in the Appendices.

We present all our photometry and magnitudes on the AB zero-point system (Oke & Gunn 1983; Fukugita et al. 1996). This includes the near-infrared, as well as the mid-infrared magnitudes. These magnitudes are *not* Galactic extinction corrected. We use a flat ΛCDM cosmology with $H_0 = 67.7$ km s^{-1} Mpc^{-1}, $\Omega_M = 0.307$, and $\Omega_\Lambda = 0.693$ Planck Collaboration (2016) to be consistent with Bañados et al. (2016) and all logarithms are to the base 10.

2 METHOD AND DATA

Quasars are generally identified by photometric selection followed by spectroscopic confirmation. Here, we reverse this method obtaining first a list of spectroscopic quasars and then obtain photometric information.

We have compiled a list of 463 quasars with redshifts $z \geq 5.00$. We use all the $z \geq 5.00$ quasars that have been discovered, spectroscopically confirmed and published as of 2018 December 31 (MJD 58483). We then obtain optical, near-infrared and mid-infrared photometry for the spectral dataset. The near-infrared data comes from two sources: first, the WFCAM (Casali et al. 2007) on the UKIRT, primarily, but not exclusively, as part of the UKIRT Infrared Deep Sky Survey (UKIDSS; Lawrence et al. 2007). And second, data from the VIRCAM on the VISTA (Emerson et al. 2006; Dalton et al. 2006). The mid-infrared, $\lambda = 3 - 30\mu$m wavelength data is from the Wide-Field Infrared Survey Explorer (WISE; Wright et al. 2010; Cutri 2013) mission. For reference, Figure 1 displays the wavelength and normalised transmission of the filters in question.

[2] wise2.ipac.caltech.edu/docs/release/allwise/expsup/sec2_1.html
[3] lsst.org; [4] sci.esa.int/euclid; [5] jwst.nasa.gov; [6] sci.esa.int/jwst; [7] www.asc-csa.gc.ca/eng/satellites/jwst; [8] jwst.stsci.edu.

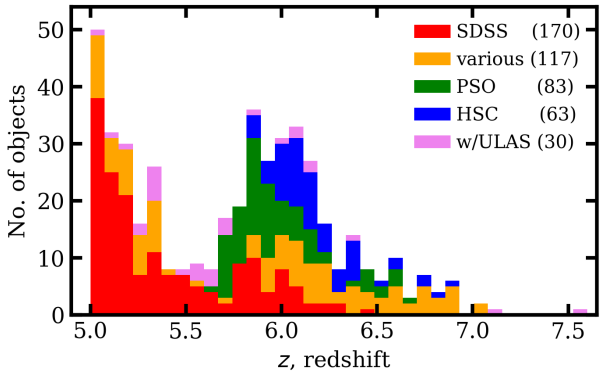

Figure 2. The redshift distribution $N(z)$ of the VHzQ sample. The bins are $\delta z = 0.075$ in width and have the data stacked on top of each other.

2.1 Spectroscopy

We compile the list of all known, spectroscopically confirmed quasars from the literature. This list was complied from a range of surveys and papers. Specifically, we use data from: Bañados et al. (2014, 2016, 2018), Becker et al. (2015), Calura et al. (2014), Carilli et al. (2007, 2010), Carnall et al. (2015), Cool et al. (2006), De Rosa et al. (2011), Fan et al. (2000, 2001b, 2003, 2004, 2006b, 2018), Goto (2006), Ikeda et al. (2017), Jiang et al. (2008, 2009, 2015, 2016), Kashikawa et al. (2015), Koptelova et al. (2017), Kim et al. (2015, 2018), Kurk et al. (2007, 2009), Leipski et al. (2014), Mahabal et al. (2005), Matsuoka et al. (2016, 2018a,b), Mazzucchelli et al. (2017), Morganson et al. (2012), Mortlock et al. (2009, 2011), McGreer et al. (2006, 2013), Reed et al. (2015, 2017), Stern et al. (2007), Tang et al. (2017), Venemans et al. (2007, 2012, 2013, 2015b,a, 2016), Wang et al. (2016, 2017, 2018a,b), Willott et al. (2007, 2009, 2010, 2013, 2015), Wu et al. (2015) Yang et al. (2018a,b) and Zeimann et al. (2011).

Most of these objects are easily identified by their broad Lyα emission line, N v emission and characteristic shape blueward of 1215Å in the rest-frame. As we shall see, some of the recently discovered objects are close to the galaxy luminosity function characteristic luminosity M^*, and some have relatively weak or maybe even completely absorbed Lyα (e.g. Figures 7 and 10 in Bañados et al. 2016). We leave aside detailed investigation and discussion into spectral features and line strengths, and take as given the published spectra and redshift identifications.

The breakdown of how many VHzQ each survey reports is given in Table 1. The Sloan Digital Sky Survey (SDSS) and the Pan-STARRS1 (PS1; PSO in Table 1) survey and alone identified over half (54.6%) of the VHzQ population. Data from the Hyper Suprime-Cam (HSC) on the Subaru telescope is responsible for 13.6% of our dataset (HSC+SHELLQs in Table 1). The combination of surveys is also vital for identifying VHzQs. The UKIDSS Large Area Survey (ULAS) on its own, or in combination with other surveys is responsible for 6.5% of the sample (SUV+ULAS) including the highest-z object. Where more than one survey is used for the high-redshift identification (e.g. via shorter-band veto and longer wavelength detection) we follow the discovery paper naming convention.

The redshifts for the VHzQs generally come from the measurement of broad UV/optical emission lines. There are far infra-red emission lines e.g. C II 158 μm available for several objects, but at the level of our current analysis broadline redshifts are sufficient.

The number of objects at or above various redshifts, along with the corresponding age of the Universe is given in Table 2.

The $N(z)$ redshift histogram is given for the sample in Figure 2. We split the contribution up by survey. For clarity we show the individual surveys of SDSS, PS1, HSC, the ULAS detection, and tally the remaining surveys together ("various").

Survey	# VHzQs	(%)	Survey reference
ATLAS	4	(0.86)	Shanks et al. (2015)
CFHQS	20	(4.32)	Willott et al. (2007)
DELS[a]	16	(3.46)	Dey et al. (2018)
ELAIS	1	(0.22)	Väisänen et al. (2000)
FIRST	1	(0.22)	Becker et al. (1995)
HSC	8	(1.73)	Miyazaki et al. (2018)
IMS	5	(1.08)	Kim et al. (2015)
MMT	12	(2.59)	McGreer et al. (2013)
NDWFS	1	(0.22)	Jannuzi & Dey (1999)
PSO	83	(17.93)	Kaiser et al. (2002, 2010)
RD	1	(0.22)	Mahabal et al. (2005)
SDSS	170	(36.72)	Stoughton et al. (2002)
SDWISE[b]	27	(5.83)	Wang et al. (2016)
SHELLQs	55	(11.88)	Matsuoka et al. (2016)
SUV[c]	20	(4.32)	Yang et al. (2017)
UHS	1	(0.22)	Wang et al. (2017)
ULAS	10	(2.16)	Lawrence et al. (2007)
VDES[d]	17	(3.67)	Reed et al. (2017)
VHS	1	(0.22)	Wang et al. (2018b)
VIK	9	(1.94)	Edge et al. (2013)
VIMOS	1	(0.22)	Le Fèvre et al. (2003)

Table 1. The source and number of the VHzQ, with the key survey reference also given. Recent survey name and acronyms include: [a]DESI Legacy Imaging Survey; [b]SDWISE = SDSS+WISE; [c]SUV = SDSS-ULAS/VHS; [d]VDES = VHS/VIKING+DES;

$z \geq$	Age / Myr	No. of objects
5.00	1180	463
5.70	1000	267
6.00	937	170
6.19	900	86
6.50	845	40
6.78	800	14
7.00	767	4
7.50	700	1

Table 2. The number of objects at or above a given redshift. The age of the Universe in Megayears is also given.

2.2 Near-infrared photometry

The near-infrared data in this paper comes from the Wide Field Astronomy Unit's (WFAU) Science Archives for UKIRT-WFCAM, the WFCAM Science Archive (WSA; Hambly et al. 2008) and VISTA-VIRCAM, the VISTA Science Archive (VSA; Cross et al. 2012). These archives were developed for the VISTA Data Flow System (VDFS Emerson et al. 2004).

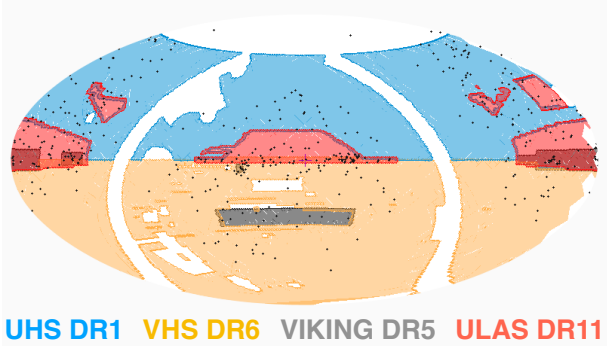

Figure 3. The coverage maps for VHS (DR6; orange), UHS (DR1; olive), VIKING (DR5; blue) and ULAS (DR11; red), the most recent public releases of the 4 main surveys. The VHzQs are given by black dots.

We access both the WSA and the VSA and include all non-proprietary WFCAM data, which covers all public surveys and PI projects from Semester 05A (2005-05-01) to 2017-Jan-01, and all non-proprietary VISTA data, which covers all public surveys and PI projects from science verification on 2009-Oct-15 to 2017-Jan-01.

Here we are not just querying the WSA or VSA data tables. We are taking a list of objects (positions) are performing matched aperture ("forced") photometry on the NIR imaging data. As such, we generate a set of tables that are different in subtle ways to the regular "Detection" tables. The two most important tables for our needs are the `[w/v]serv1000MapRemeasurement` and `[w/v]serv1000MapRemeasAver`.

We produce and provide a two new databases with all the necessary quantities and measurements to fully reproduce our tables, figures and results herein. Moreover, these databases report considerably more information than we report here. Full documentation can be found at the WSA Schema Browser and the VSA Schema Browser.

Figure 3 shows the areal coverage of the ULAS, UHS, VHS and VIKING. UHS DR1 is 12,600 deg^2 (J-band); ULAS DR11 3,700 deg^2 VHS DR6 16,000 deg^2 and VIKING DR5 is 1,300 deg^2. The overlap between UHS DR1 and VHS DR6 is 28 deg. These four surveys together cover 33,000 deg^2.

2.2.1 Averaging matched photometry

The data was processed using a matched-aperture photometry method where flux is measured at the spectroscopic position of the quasar, without necessarily knowing if there is a formal detection in the NIR photometry beforehand. The matched-aperture pipeline is discussed in Cross et al. (2013) and with fuller details to appear in a forthcoming paper (Cross et al., 2019, in prep).

We query the WSA and VSA performing matched-aperture photometry at the positions of our 463 VHzQs. This database is world-readable and we give the full recipe and relevant SQL queries for accessing both databases in Appendix B as well as online.

The photometry in a single epoch image often has low signal-to-noise. The advantage of matched aperture photometry on quasars is that co-adding is relatively simple if each epoch is taken in the same aperture and the aperture photometry has been corrected to total. Indeed, the standard aperture corrections work well for point sources. Coadding using the matched-aperture photometry can give better results for the photometry, where the individual epochs are taken from multiple projects with different field-centres and orientations and point-spread functions since the individual epoch scattered light, pixel distortion and aperture corrections can be applied with the correct weighting.

We average the aperture corrected calibrated fluxes (e.g. **aperJky3**), and then convert to magnitudes.

$$\bar{F} = \frac{\sum_i^N (w_i\, F_i)}{\sum_i^N w_i} \tag{1}$$

where F_i is the i^{th} epoch measurement of a parameter to be averaged such as the aperture corrected calibrated flux in a $1''$ aperture (**aperJky3**) and $\bar{F}$ is the weighted mean average of this parameter. The weight for each epoch $w_i = 1/(\sigma_F)^2$ if the epoch is included and $w_i = 0$ if an epoch is excluded for quality control purposes. The weights of each epoch in each averaged catalogue are tabulated in the `[w]serv1000MapAverageWeights`.

We calculate a set of averaged catalogues, for each pointing and filter, based on the requirements in `RequiredMapAverages`, in these cases over time spans of 7, 14, 30, 91, 183 days, 365 days, 730 days, over 10 epochs and over all epochs. The averaging process starts at the first epoch and works onwards from there. Again, we present these measurements in the new SQL tables.

We detect 359 unique quasars in the WFCAM WSA database, 220 quasars are detected in the VISTA VSA database with 130 objects in common with both WFCAM and VISTA data. We give the necessary SQL queries syntax at `d80b2t/VHzQ`.

2.3 MIR data

The MIR data for this study comes from the Wide-field Infrared Survey Explorer (WISE) mission, and we utlize data from the WISE cryogenic and the Near-Earth Object WISE (NEOWISE; Mainzer et al. 2011) post-cryogenic and NEOWISE Reactivation Mission (NEOWISE-R Mainzer et al. 2014) survey phases.

We use data from the beginning of the WISE mission (2010 January; Wright et al. 2010) through the fifth-year of NEOWISE-R operations (Mainzer et al. 2011, 2018 December;). There are several major data releases and catalogues based on the WISE mission. Here we use two: the WISE AllWISE Data release and the recently released "unWISE Catalog" Schlafly et al. (2019). The AllWISE program combines the W1 and W2 Single-exposure data from all the WISE survey phases (4-Band Cryo, 3-Band Cryo and Post-Cryo; 2010-01-07 thru 2011-02-01) survey phases, and the W3 and W4 from the 4-Band Cryo phase. The unWISE effort[9] is the unblurred coadds of the WISE imaging using the AllWISE and NEOWISE-R stacked data (Lang 2014; Meisner et al. 2018a,b).

For the two shorter WISE bands, $\lambda_{\rm eff} 3.37\mu$m W1 and

[9] http://unwise.me

$\lambda_{\rm eff}4.62\mu$m W2 we generally report the deeper, unblurred unWISE coadd data. For the two longer WISE bands, $\lambda_{\rm eff}12.1\mu$m and $\lambda_{\rm eff}22.8\mu$m we use the AllWISE Data Release. Most objects in the AllWISE Source Catalog are unresolved, so the best photometric measurements to use are the deep detection profile-fit photometry measures, `wxmpro`, `wxsigmpro` and `wxsnr`. The unWISE Catalog absolute photometric calibration derives from the photometric calibration of the unWISE coadds (Meisner et al. 2017), which is tied to the original WISE zero points through aperture fluxes in a 27.5" radius. Critically, we also note that

Previous works (e.g., Krawczyk et al. 2013; Ross et al. 2015; Bilicki et al. 2016) found that cross-matches performed with a radius of 2-3" between the user catalogue and WISE was a good compromise between completeness and contamination (see e.g. Figure 4 of Krawczyk et al. 2013). We thus use a cross-match radius of 2.75". When querying the AllWISE catalogues, "Cone Search Radius" in the AllWISE table search was set to 2.75" for the Spatial Constraints. The "One to One Match" was "not" checked; although possible, we consider it highly unlikely there would be more than one MIR source contributing to the flux of a single UV/optically bright rest-frame quasar. Investigating this in detail is very interesting but left to a future study.

Knowing we have secure detections in the near-infrared bands, and wanting to boost the number of WISE W3/W4 detections, we allow ourselves to be less conservative in querying the AllWISE catalogues and also query the AllWISE Reject Table. However, with the exception of one object (SHELLQs J1208-0200), the AllWISE Reject Table does not contain any further W3/W4 detection information.

All fluxes in the unWISE catalog are reported there are in "Vega nanoMaggies", with the Vega magnitude of a source is given by

$$m_{\rm Vega} = 22.5 - 2.5\log(f), \quad (2)$$

where f is the source flux. The absolute calibration for unWISE is ultimately inherited from AllWISE through the calibration of Meisner et al. (2017). This inheritance depends on details of the PSF normalization at large radii, which is uncertain. Subtracting 4 millimag from the unWISE W1, and 32 millimag from unWISE W2 fluxes improves the agreement between unWISE and AllWISE fluxes.

Thus to convert unWISE Vega magnitudes onto the AB system, we have:

$$\begin{aligned} {\rm W1}_{\rm AB,unWISE} &= 22.5 - 2.5\log(f_{\rm W1}) - 0.004 + 2.699 \\ {\rm W2}_{\rm AB,unWISE} &= 22.5 - 2.5\log(f_{\rm W2}) - 0.032 + 3.339. \end{aligned}$$

For the our MIR variability investigations, we do not use the unWISE coadds, but instead use the AllWISE catalogue and the NEOWISE 2019 Data Release. NEOWISE 2019 makes available the 3.4 and 4.6 m (W1 and W2) single-exposure images and extracted source information that was acquired up until 2018 December 13 (MJD 58465) including the fifth year of survey operations of NEOWISE. These fifth year NEOWISE data products are concatenated with those from the first four years into a single archive from 2013 December 13 (MJD 56639).

The WISE scan pattern leads to coverage of the full-sky approximately once every six months (a"sky pass"), but the satellite was placed in hibernation in 2011 February and then reactivated in 2013 October. Hence, our light curves have a cadence of 6 months with a 32 month sampling gap.

Table 3 represents the culmination of this effort, and we now exam the assembly of its contents in more detail.

Survey	QsoName	R.A. / deg (J2000)	Decl. / deg (J2000)	redshift	Z	Y	J	H	K	
PSO	J000.3401+26.8358	0.34011	26.83588	5.75	-1000.00 ± -1000.000	-1000.00 ± -1000.000	19.28 ± 0.062	-1000.00 ± -1000.000	-1000.00 ± -1000.000	16.28
SDSS	J0002+2550	0.66412	25.84304	5.82	-1000.00 ± -1000.000	-1000.00 ± -1000.000	19.37 ± 0.069	-1000.00 ± -1000.000	-1000.00 ± -1000.000	16.25
SDWISE	J0008+3616	2.21429	36.27041	5.17	-1000.00 ± -1000.000	-1000.00 ± -1000.000	19.33 ± 0.063	-1000.00 ± -1000.000	-1000.00 ± -1000.000	16.01
PSO	J002.3786+32.8702	2.37870	32.87026	6.10	-1000.00 ± -1000.000	-1000.00 ± -1000.000	20.99 ± 0.249	-1000.00 ± -1000.000	-1000.00 ± -1000.000	17.95
SDSS	J0012+3632	3.13700	36.53781	5.44	-1000.00 ± -1000.000	-1000.00 ± -1000.000	19.01 ± 0.049	-1000.00 ± -1000.000	-1000.00 ± -1000.000	15.82
PSO	J004.3936+17.0862	4.39361	17.08630	5.80	-1000.00 ± -1000.000	-1000.00 ± -1000.000	20.56 ± 0.202	-1000.00 ± -1000.000	-1000.00 ± -1000.000	17.83
PSO	J006.1240+39.2219	6.12404	39.22193	6.62	-1000.00 ± -1000.000	-1000.00 ± -1000.000	21.28 ± 0.422	-1000.00 ± -1000.000	-1000.00 ± -1000.000	17.36
SDWISE	J0025-0145	6.36183	-1.75903	5.07	-1000.00 ± -1000.000	-1000.00 ± -1000.000	-1000.00 ± -1000.000	17.74 ± 0.004	-1000.00 ± -1000.000	14.85
PSO	J007.0273+04.9571	7.02733	4.95712	6.00	-1000.00 ± -1000.000	20.33 ± 0.056	20.23 ± 0.074	20.29 ± 0.108	20.19 ± 0.105	17.17
SDWISE	J0031+0710	7.85775	7.17692	5.33	-1000.00 ± -1000.000	20.03 ± 0.082	20.20 ± 0.146	19.49 ± 0.106	19.61 ± 0.123	16.65
SDSS	J0034+3759	8.55979	37.99833	5.63	-1000.00 ± -1000.000	-1000.00 ± -1000.000	19.70 ± 0.091	-1000.00 ± -1000.000	-1000.00 ± -1000.000	16.48
PSO	J011.3899+09.0325	11.38987	9.03249	6.42	-1000.00 ± -1000.000	21.04 ± 0.234	-1000.00 ± -1000.000	20.64 ± 0.177	20.76 ± 0.251	17.77
CFHQS	J0050+3445	12.52777	34.75601	6.25	-1000.00 ± -1000.000	-1000.00 ± -1000.000	19.97 ± 0.120	-1000.00 ± -1000.000	-1000.00 ± -1000.000	16.58
SDSS	J0054-0109	13.58925	-1.15600	5.09	-1000.00 ± -1000.000	19.60 ± 0.057	19.39 ± 0.065	19.22 ± 0.078	19.59 ± 0.116	16.98
CFHQS	J0055+0146	13.76212	1.77175	6.01	-1000.00 ± -1000.000	24.12 ± 2.525	23.03 ± 1.443	22.38 ± 1.334	21.08 ± 0.374	-99.99
SDSS	J0056+2241	14.23350	22.68671	5.49	-1000.00 ± -1000.000	-1000.00 ± -1000.000	19.99 ± 0.099	-1000.00 ± -1000.000	-1000.00 ± -1000.000	16.93
SDSS	J0100+2802	15.05426	28.04053	6.33	-1000.00 ± -1000.000	-1000.00 ± -1000.000	17.60 ± 0.012	17.48 ± 0.018	-1000.00 ± -1000.000	14.44
SDUV	J0108+0711	17.02750	7.18906	5.53	-1000.00 ± -1000.000	19.96 ± 0.070	19.82 ± 0.088	19.55 ± 0.089	19.56 ± 0.093	16.33
SDSS	J0108-0100	17.12483	-1.00433	5.11	-1000.00 ± -1000.000	20.91 ± 0.191	21.93 ± 0.621	20.96 ± 0.353	21.01 ± 0.432	-99.99
SDUV	J0113+0559	18.47396	5.99753	5.00	-1000.00 ± -1000.000	20.34 ± 0.094	20.21 ± 0.118	19.77 ± 0.108	19.62 ± 0.092	16.68
SDSS	J0114+3238	18.72962	32.63787	5.22	-1000.00 ± -1000.000	-1000.00 ± -1000.000	19.93 ± 0.096	-1000.00 ± -1000.000	-1000.00 ± -1000.000	16.84
SDWISE	J0115-0253	18.94279	-2.88673	5.07	19.88 ± 0.076	19.91 ± 0.085	19.62 ± 0.075	19.53 ± 0.087	19.50 ± 0.086	16.36
SDSS	J0120+2147	20.22471	21.78506	5.42	-1000.00 ± -1000.000	-1000.00 ± -1000.000	20.09 ± 0.101	-1000.00 ± -1000.000	-1000.00 ± -1000.000	16.54

Table 3. The first 23 (i.e. 5%) of 463 very high-z quasars with near and mid-infrared photometry.

Selection	number detected (%)
Any band ($ZYJHK/K_s$)	449 (97.0)
Z-band	75 (16.2)
Y-band	273 (59.0)
J-band	447 (96.5)
H-band	269 (58.1)
K or Ks-band	322 (69.5)

Table 4. Detection rate of VHzQs in the near-infrared. For the 14 objects that have no NIR detections, 3 have been observed but are not in our queried time range, 6 have not been observed yet and 5 objects are too far north to be visible by UKIRT.

abs(VIRCAM - WFCAM)	millimags	no. of objects
Z	23.2	3
Y	57.3	53
J	2.1	106
H	45.8	96
K_s/K	25.2	110

Table 5. Comparing the magnitudes in different WFCAM/UKIRT and VIRCAM/VISTA near-infrared bands.

$z \geq$	unWISE		AllWISE	
	W1	W2	W3	W4
5.00	362 (78.2%)	308 (66.5%)	51 (11.0%)	10 (2.2%)
5.70	186 (69.4%)	151 (56.3%)	15 (5.6%)	2 (0.7%)
6.00	109 (63.7%)	91 (53.2%)	8 (4.7%)	2 (1.2%)
6.19	63 (72.4%)	47 (54.0%)	3 (3.4%)	2 (2.3%)
6.50	34 (85.0%)	26 (65.0%)	1 (2.5%)	2 (5.0%)
6.78	12 (85.7%)	9 (64.3%)	0 (0.0%)	0 (0.0%)
7.00	4 (100.0%)	4 (100.0%)	0 (0.0%)	0 (0.0%)
7.50	1 (100.0%)	1 (100.0%)	0 (0.0%)	0 (0.0%)

Table 6. Detection rates in the mid-infrared bands from WISE as a function of redshift. A signal-to-noise cut of `wxsnr`> 3.0 has been used for each band.

3 RESULTS

Having collated the sample of 463 VHzQs, and obtained their near- and mid-infrared photometry we report here the various photometric properties of the quasars.

First, we will concentrate on detection rate in the infrared, go on to report on the colour-redshift and colour-colour properties of our sample and then report on how the current sample populates the luminosity-redshift Lz-plane.

3.1 Detection Rates in the NIR

Table 4 gives the detection rates for the VHzQs in the NIR $YJHK/K_s$-bands. The first thing to note is that the coverage of the NIR surveys for example from the UKIDSS LAS and VISTA VHS, does not overlap the full area for where the VHzQs are detected.

There are 14 objects that have no NIR detections. 3 of these (PSOJ053.9605-15.7956, PSO J056.7168-16.4769 and DELSJ0411-0907) have been observed (by VHS) but are out of our queried time range (for which the data is publicly available). 6 objects are at declination $\delta < 0$ deg and have not been observed (or at least the data is not in the VSA archive yet). 5 objects are at a declination $\delta \geq +60$ deg are too far north for UKIRT and cannot be observed.

We note that although we are often working close to the magnitude limits of the surveys, Eddington bias is not a significant effect on our measurements, since we are not discovering new sources, but measuring properties of already known quasars. Indeed in the NIR WFCAM/VISTA data, using forced photometry reducing the Eddington bias to negligible levels since a flux will be measured regardless of whether the source is just bright enough or too faint to be detected above the background noise.

3.1.1 Comparing WFCAM and VISTA

There are 130 quasars observed in the overlapping area between WFCAM and VISTA. We used the `VegaToAB` values to put these objects on the same AB system, and for each object compared the two measurements. First, we calculated the weighted average (calibrated flux) in each filter of both and calculated the ratio and difference between each measurement and the average. Then for each filter we calculated the weighted average of the differences (in mag) for each instrument to see if there were significant offsets. The results are given in Table 5. The only filter with a significant offset is the Y-band. All of the VISTA averages are negative and all of the WFCAM ones are positive. The Ks versus K band comparison may be affected the different shapes of the filters, with K being significantly wider than K_s, able to detect light at longer wavelengths.

We have also checked for quasars with large differences in magnitude between the WSA and VSA. Objects were selected where the average flux was $> 0.$ and > 5 average flux error. In order to account for large errors in either the WFCAM or VISTA photometry, objects with δmag$< 2\times \sigma_{\delta\mathrm{mag}}$ in either WSA or VSA were removed. This selects two quasars with large, δmag > 0.2mag differences between the WSA and VSA. These are SDSSJ0349+0034 and SDSSJ2220-0101. For SDSSJ0349+0034 has a WSA K-band magnitude of 19.13 ± 0.24, while for the VSA K_s-band this is 18.36 ± 0.10 mag. For SDSSJ2220-0101, in J-band WSA = 22.23 ± 0.15, for the VSA = 19.38 ± 0.04.

3.2 Detection Rates in the MIR

Unlike the NIR coverage, the WISE satellite and mission performed an all-sky survey, so the location of every VHzQ in our dataset is covered. However, the depth of the WISE survey depends heavily on sky location, with locations near the Ecliptic Poles having the highest number of exposures.

Before reporting on the detection rates, we investigate this effect using the AllWISE Source Catalog. Figure 4 shows the WISE ALLWISE magnitude versus signal-to-noise, colour coded by `wxcov` the mean coverage depth, in each corresponding band. The `w123cov` values are the mean pixel coverage in W1/2/3 from the W1/2/3 Atlas Tile Coverage Map within an aperture of circular area with a radius of 8.25" centered on the position of this source. For `w4cov` this radius is 16.5" (the AllWISE Source Catalog Column Descriptions has further details). The `wxcov` value takes into account e.g., individual pixels in the measurement area that may be masked or otherwise unusable (reducing the effective pixel count and thus the mean coverage value) as well as

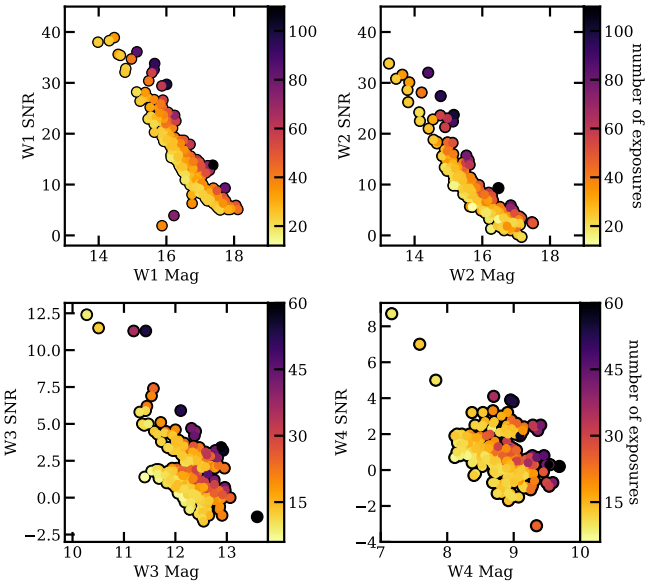

Figure 4. WISE W1/2/3/4 `wxmpro` magnitude against signal-to-noise, colour coded by `wxcov` the mean coverage depth, in each corresponding band.

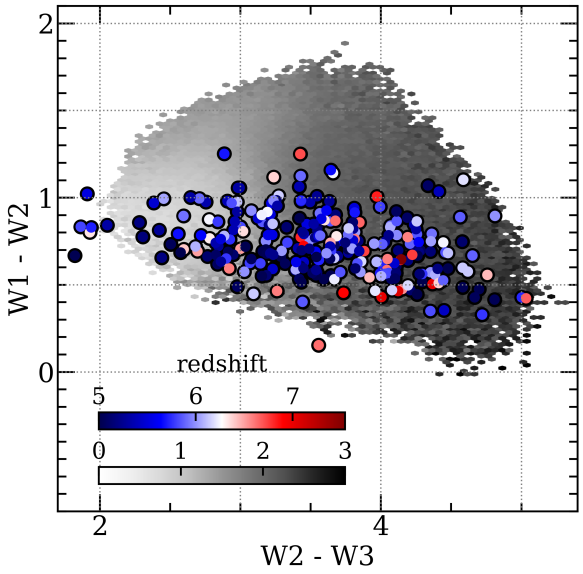

Figure 5. The (W2-W3) vs. (W1-W2) colour colour diagram showing the WISE colours for the 283 VHzQ that have reported w3mpro values (blue to red coloured points). 400,000 quasars at redshift $z \lesssim 3.0$ from the DR14Q are also shown (grey colour-scale).

pixels that are affected by distortions across the across the focal plane in single-exposure images (where this distortion is corrected when coadding to generate the Atlas Images). In the two shorter bands W1/2 we see the clear and expected trend for brighter objects to have larger SNR, and also for the higher signal to noise for objects with more exposures at a given magnitude. The behaviour for the W3/4 bands is different, with two populations clearly evident in W3 and although a bit more mixed, also in W4. With the suggested split at SNR> 2, and no obvious R.A./Declination dependence seen, this behaviour is explained by the fact that there are non-detections in W3/4 for objects (with high W1/2 SNR) that are reported in the ALLWISE catalogue.

Table 6 gives the detection rates for the VHzQs in the MIR WISE W1-4 bands. The unWISE depths are impressive with nearly 80% of all the VHzQs being detected in unWISE W1. 12 out of 14 (86%) in unWISE W1 (9 our of 14; 64% in unWISE W2) of the $z \geq 6.78$ quasars are detected and moreover *all of the* $z \geq 7$ *quasars are detected in both unWISE W1 and W2*. This bodes very well for future, small mirror infrared missions (e.g. Ross et al. 2019).

Recently, Assef et al. (2018) released two large catalogues of AGN candidates identified across 30,000 deg^2 of extragalactic sky from the WISE AllWISE Data Release. The "R90" catalogue, contains 4.5M AGN candidates at 90% reliability (and ≈150 AGN candidates per deg^2) while the "C75" catalogue consists of 20.9M AGN candidates at 75% completeness (and (≈700 AGN candidates per deg^2). Cross-matching our catalogue of 463 VHzQs with these catalogues, produces 42 matches with the R90 sample and 98 matches with the C75 sample. Both catalogues unsurprisingly match to the ultraluminous quasar SDSS J0100+2802 (Wu et al. 2015) while the C75, but not the R90 catalogue matches to the first redshift $z > 7$ quasar ULAS J1120+0641 (Mortlock et al. 2011). Neither catalogue matches to the current highest-redshift object J1342+0928 (Bañados et al. 2018).

3.3 MIR Colours

Due to the depth all-sky coverage of the WISE (and NEOWISE-(R)) mission, several investigations have looked at how WISE detects AGN Stern et al. (e.g 2012); Assef et al. (e.g 2012); Secrest et al. (e.g 2015); LaMassa et al. (e.g 2017); Assef et al. (e.g 2018); Glikman (e.g 2018); LaMassa et al. (e.g 2019)

The VHzQ with the bluest colour in (W1 - W2) is DELS J1048-0109 with (W1-W2) = 0.154.

Figure 5 shows the (W1-W2) vs. (W2-W3) colour colour space diagram showing the WISE colours for the 283 VHzQ that have reported `w3mpro` values (blue to red coloured points), though we note that only 51(18%) of these objects have `w3snr` ¿ 3.0. objects 400,000 quasars at redshift $z \lesssim 3.0$ from the DR14Q are also shown (grey colour-scale).

The set of VHzQ detected in WISE W3 and W4 contains 51 objects that are detected in the broad W3 filter and 10 objects that are formally detected in W4 (`w4snr`≥3.0). Four of the brightest W4 objects are presented in . UHS J0439+1634 (Fig. 6 (a)) with W4=7.165±0.12 was discovered by Fan et al. (2019b) and is a strongly lensed quasar at z =6.51. This high luminosity is mostly not intrinsic, but is boosted by an intervening redshift z ∼0.7 galaxy. SDSS J0100+2802 (redshift $z = 6.33$) does not have a formal W4 detection (W4 = 8.98±0.45 and `w4snr`=2.4), but as reported by Wu et al. (2015), has a bright detection in the 2MASS J, H and K_s bands and we report it here. Other high-redshift quasars that are bright W3/4 objects may well also so be lensed (e.g., Glikman et al. 2018; Fan et al. 2019b), but high-resolution follow-up is needed to confirm.

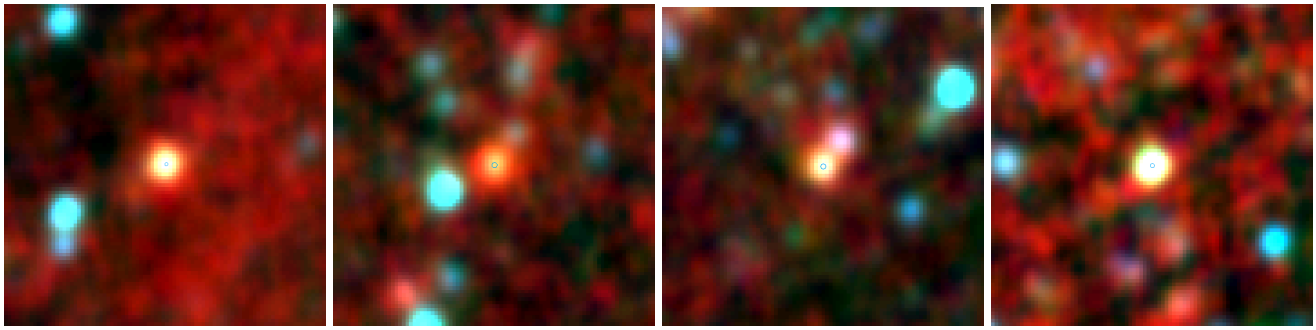

Figure 6. Four of the brightest MIR VHzQs. The thumbnails are the RGB colour outputs using the ALLWISE W1W2W3 bands from the IRSA WISE Image Service, with a scale of 120" on the side. *(a)* UHS J0439+1634 was discovered by Fan et al. (2019b) and is a strongly lensed quasar at z =6.51. *(b)* SDSS J0100+2802 is the Wu et al. (2015) object. *(c)* SDSS J1443+3623 has `w3mpro, w4mpro` = (11.189 ± 0.1, 8.699 ± 0.26) and *(d)* SDSS J1623+4705 has `w3mpro, w4mpro` = (11.425 ± 0.1, 8.954 ± 0.28).

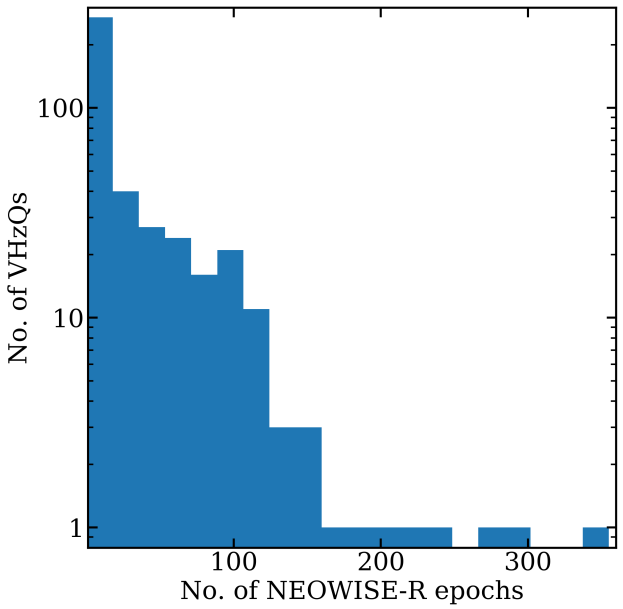

Figure 7. Histogram showing the total number of exposures for each detected VHzQ from the full combination of ALLWISE, NEOWISE and NEOWISE-R.

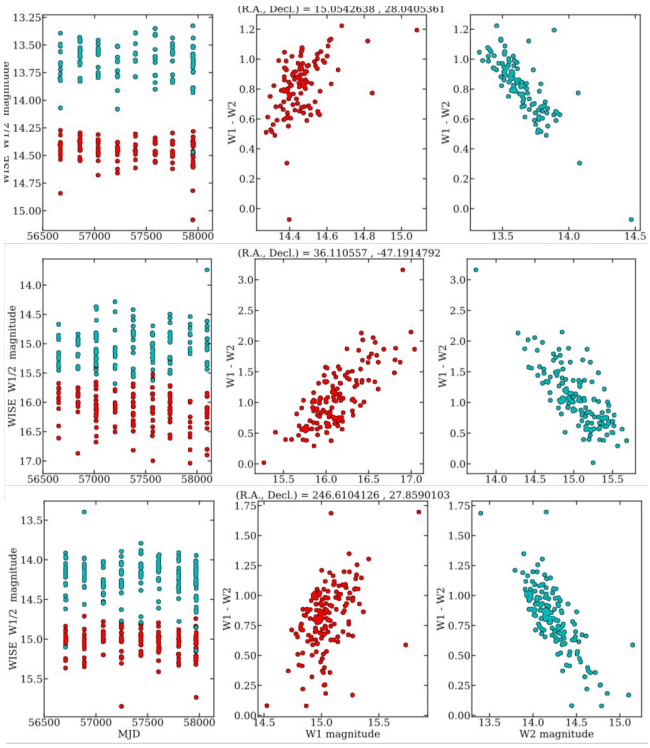

Figure 8. Here we show the MIR NEOWISE-R for J0100+2802 (Wu et al. 2015), J0224-4711 and J1626+2751. Red points are the W1 band; cyan points the W2 band.

3.4 Variability

VHzQs, if accreting at, or above the Eddington limit, might well have changing mass accretion rates, i.e., $\dot{m}_{\rm accr}$. A consequence of this would be that these quasars exhibit signs of variability, most likely showing up in their UV/optical rest-frame emission. We look for evidence of this variability signature in the NIR and MIR light-curves of the VHzQs.

Quasars are known to have dramatically changing Balmer lines, especially Hβ (e.g., LaMassa et al. 2015; Ruan et al. 2016; Runnoe et al. 2016; MacLeod et al. 2016; Gezari et al. 2017; Runco et al. 2016; Yang et al. 2018c; Assef et al. 2018; Stern et al. 2018; Ross et al. 2018; MacLeod et al. 2019; Graham et al. 2019). As a guide, we note that Hα is redshifted to 3.94μm (i.e. W1) at z = 5.00 and 5.57μm, which is between the W2 and W3-bands at z = 7.50. Hβ is redshifted to 2.92μm, which is the blue edge of W1, at z = 5.00 and 4.13μm at z = 7.50. Less well understood is the temporal behaviour of the metal lines, in particular C IV and Mg II . C IV enters the Y-band at redshift z=5.32 and exits at z=5.99, and enters the J-band at redshift z = 6.55 and exits at z=7.57. Mg II enters the H-band at redshift z = 4.33 and exits at z = 5.37 and enters the K-band at redshift z = 6.25 and exits at 7.50.

One key point to note when looking at the WISE variability is that It's just that the NEOWISE-AllWISE match radius is 3": AllWISE and 2MASS source information included in the NEOWISE Source Database are associations not identifications.

Figure 7 gives the number of NEOWISE-R epochs and detections there are for each VHzQ, while Figure 8 presents three examples of the MIR lightcurves and associated colour

changes. Here we show J0100+2802 (Wu et al. 2015), J0224-4711 and J1626+2751.

Using the extended datasets described in Section 2.2, we select objects with at least 8 measurements observed with intervals of at least 30 days, in at least one filter. The the average calibrated flux over all epochs must be > 0 (i.e. `aperJky3`> 0) with the signal-to-noise is required to be ≥ 8 (i.e. `aperJky3/aperJky3Err`$\geq$8). With these criteria, there are 21 WFCAM and 12 VISTA objects with 1 object (VIK J1148+0056) in common to both, and this sample of 32 is our starting point for variability investigations.

The clipped median and median absolute deviation is then calculated

$$var = 1.48 \times \text{m.a.d.}/\bar{\epsilon} \quad (3)$$

where var is the index of variation, m.a.d. is the median absolute deviation, and $\bar{\epsilon}$ is the mean of the error in each point in the light curve, divided by the total number of points. We apply the criteria $var >= 3.$ to light-curves from the original measurements and also to light-curves where measurements have been averaged over different time-scales to improve the signal-to-noise. We found that two quasars showed signs of variability: MMT J0215-0529 (see Fig. 9) in the Y-band with an average time-scale of 30 days and amplitude of 0.3 mag, and SDSS J0959+0227 (see Fig. 12) in the Y and H-bands, with timescales of 1 year or 6 months for Y only. The H-band amplitude was 0.9 mag and the Y-band amplitude was 1.2 mag if averaged over 6 months, or 0.9 mag if averaged over 1 year.

We present four objects that are particularly well-sampled in the NIR. These are: MMT J0215-0529 ($z = 5.13$; Figure 9), CFHQS J0216-0455 ($z = 6.01$; Figure 10), SHELLQs J0220-0432 ($z = 5.90$; Figure 11) and SDSS J0959+0227 ($z = 5.07$; Figure 12). We incorporate the MIR NEOWISE-R light curve data where available.

We note that sometimes the average flux is negative and so a default magnitude is reported. This is apparent for the average H and K_s flux for CFHQS J0216-0455 at MJD=56900. Interestingly this is evident in both the H and K_s filters, but with this quasar not much brighter than the detection limit, one must be very careful with any (over) interpretation.

Even with well sampled data across the 3000-4000 day observed time-scales that the WFCAM and VISTA surveys span, the $(1+z)$ time-dilation dramatically affects the sampled rest-frame timescales sampled, which are $\sim 300-700$ days. Indeed, when sharp changes in a accretion rate are expected on the system's dynamical timescale of several kilo-years (e.g., Regan et al. 2019), then seeing any variability signature is not expected. However, noting how in lower redshift quasars, which also have massive $> 10^8$ $M_\odot$ black holes, dramatic changes in both continuum and line emission *is seen* on much shorter timescales, continued monitoring of these objects is warranted.

We finally focus on SDSS J0959+0227 which is presented in Wang et al. (2016) but is first reported in Civano et al. (2011) as CID-2220 and a high-redshift, $z > 3$ AGN, in the Chandra-COSMOS field. The spectrum from this object is presented in Ikeda et al. (2012) and shows SDSS J0959+0227 having a narrow Lyα line, and would likely be a Lyman-α emitting galaxy had it not been an X-ray source, The X-ray luminosity is $\approx 3\times10^{44}$ erg s^{-1} in the 2-10 keV

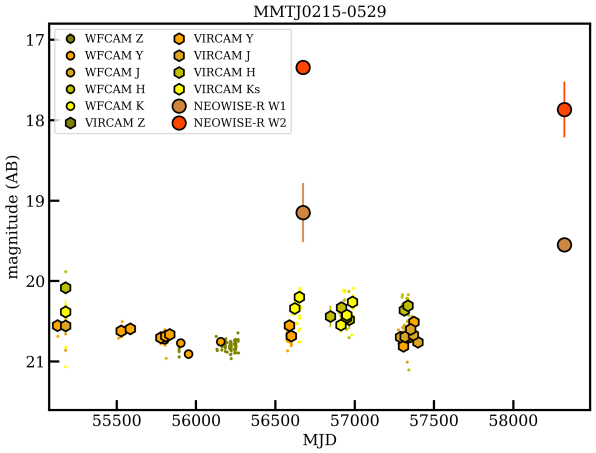

Figure 9. The infrared light curve for MMT J0215-0529 with data from WFCAM (smaller solid circles), VIRCAM (hexagons) and NEOWISE-R (larger solid circles). MMT J0215-0529 was identified by McGreer et al. (2018),

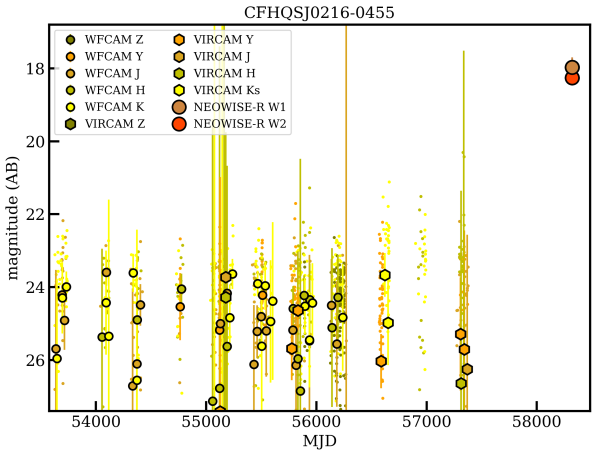

Figure 10. The same as Fig. 9 except for CFHQS J0216-0455.

rest-frame, so it is an AGN. This object is clearly not a regular broadline "Type 1" AGN. Noting that the redshift of $z = 5.07$ for SDSS J0959+0227, the Y, J, H, Ks/K-bands correspond to rest-wavelengths of ∼1690, 2055, 2690, 3515/3625Å i.e. the rest-frame UV/very blue, so, so the regular blue QSO continuum could be emerging Thus, with the slightest hint of variability, this could potentially be a high-z AGN transitioning from a narrow-line "Type 2" object to a broadline Type 1 quasar.

4 SURFACE DENSITY OF VHZQS

One interesting question to ask is given the compilation of VHzQs assembled here, are there bright $z > 5.00$ quasars that are in *current* photometric datasets, and if so, how

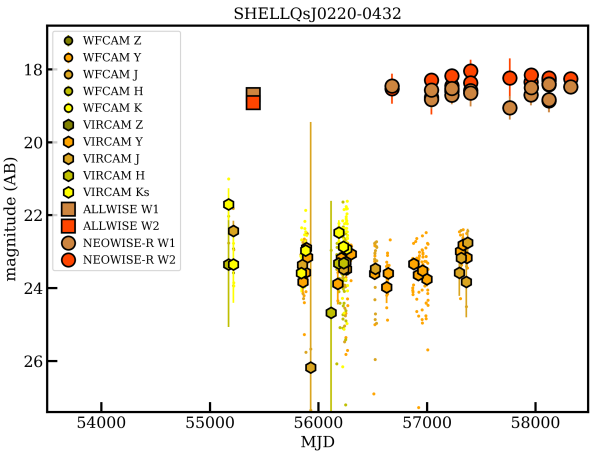

Figure 11. The same as Fig. 9 except for SHELLQs J0220-0432.

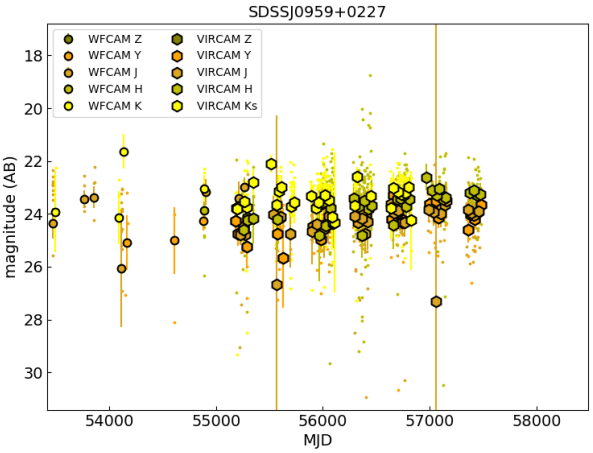

Figure 12. The near infrared light curve for SDSS J0959+0227. Note, SDSS J0959+0227 is too faint in the MIR to be detected by ALLWISE or unnWISE.

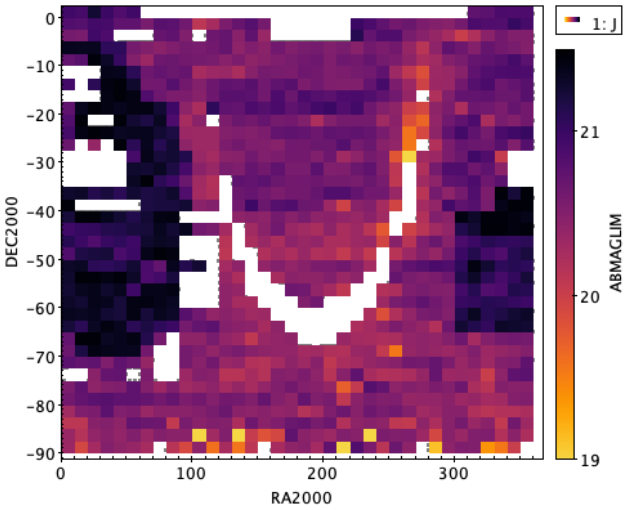

Figure 13. The calculated average `AB MAGLIM` in the VHS. As one can see, VHS is not completely uniform. The are 3 areas with different filter sets, and the depths changed in 2 of these areas, particularly in J and K_s. Y and H are almost uniform, but the coverage is much less.

many are still to be discovered and confirmed spectroscopically?

In the North, we assume the UHS J-band depth of 19.6 (Vega; Dye et al. 2018). In the South, one can use the report `ABmagLimits` for each survey in the database, we can calculate the depths of the various NIR VISTA surveys. Fig. 13 shows this calculated average `AB MAGLIM` in the VHS. As one can see, the VHS is not completely uniform. The area wrapping round 310$\lesssim$RA/deg$\lesssim$90 and -70$\lesssim$ Decl./ deg $\lesssim$ -40 has a J-band depth of 21.2 AB mag, whereas the rest of the VHS area, the J-band depth is closer to 20.6 AB mag.

Having obtained an as-near-to-homogenous set of photometry as we can, we are now in a position to calculate the Absolute Magnitudes of the VHzQ sample and in particulare the absolute magnitude at rest-frame 1450Å , M_{1450}, which is a key physical quantity and goes directly towards the quasar luminosity function and thus the reionization of hydrogen calculation.

We calculate the Distance Modulus in the normal fashion,

$$m_{1450} - M_{1450} = 5 \log \left(\frac{D_{\rm L}(z)}{\rm Mpc} \right) + 25 + K_{\rm corr}(X, z) \quad (4)$$

where m_{1450} is the apparent magnitude at 1450Å , $D_{\rm L}(z)$ is the luminosity distance and $K_{\rm corr}(X, z)$ is the K-correction which corrects for the effects of redshifting of the bandpass and the spectrum.

The m_{1450} apparent magnitude is derived from the $z-$, $y/Y-$ or $J-$band photometery. The Pan-STARSS1 $z_{\rm PS1}$ and $y_{\rm PS1}$-bands approximatley sample the redshift ranges $4.53 \leq z \leq 5.45$ and $5.28 \leq z \leq 6.47$, respectively for 1450Å' emission, while the VIRCAM $Y_{\rm VIRCAM}-$ and $J_{\rm VIRCAM}$-bands cover $5.50 \leq z \leq 6.57$ and $7.06 \leq z \leq 8.16$.

Ross et al. (2013) has a detailed discussion of the K-correction (see that papers' Appendix B). The key result in that paper is, if quasars are described as having a power-law slope, α^{ν} in spectral flux density, i.e., $f_{\nu}(\nu) \propto \nu^{\alpha_{\nu}}$ (as is conventional) then

$$K_{\rm corr}(z) = -2.5(1 + \alpha_{\nu}) \log[1 + z]. \quad (5)$$

Here the $[-2.5 \log(1+z)]$ term corrects for the effective narrowing of the filter width with redshift, (the "bandpass correction") and the $[-2.5\alpha^{\nu} \log(1+z)]$ term takes into account the spectral index correction. The bandpass correction is approximately ≈ -1.945 at redshift $z = 5$ decreasing to -2.32 at redshift $z = 7.50$.

Following Fan et al. (2001a) and McGreer et al. (2013), we use use an exponential decline to describe the space density of VHzQs at high redshifts, e.g.

$$\rho(z, {\rm M}_{1450}) \propto 10^{k(z)} \quad (6)$$

where z is the sample redshift.

5 CONCLUSIONS

In this study, we have, for the first time, compiled the list of all $z > 5$ spectroscopically confirmed quasars. We have assembled the NIR ($y/Y, J, H, K/K_s$) and MIR (WISE W1/2/3/4) photometry for these objects, given their detection rates and SEDs. We find that:

- SDSS and Pan-STARRS1 together identified over half of the VHzQ sample;
- There remains a quasar "redshift desert" at $z \approx 5.3 - 5.7$, though efforts are being made to address this (e.g., Yang et al. 2018a);
- 97.0% of the VHzQ sample is detected in one or more NIR ($ZYJHK/K_s$) band;
- The 14 objects that are not detected in the NIR are due to lack of coverage rather than lack of depth;
- 362 (78.2%) VHzQs are detected by WISE, e.g. in the deeper unWISE W1 catalog.
- All of the $z \geq 7$ quasars are detected in both unWISE W1 and W2.
- 32 of the quasars had enough NIR measurements and sufficient NIR measurements and signal-to-noise to look for variability. Weak variability was detected in multiple bands of SDSS J0959+0227, and very marginally in the Y-band of MMT J0215-0529. 2 other quasars, SDSS J0349+0034 and SDSS J2220-0101 had significant differences between their WFCAM and VISTA magnitudes in one band, also indicating variability.

The science reach of $z > 5$ quasars will continue to be important well into the next decade (Becker et al. 2019; Fan et al. 2019a; Wang et al. 2019) and will provide key insights into direct collapse black holes, hydrogen reionization and the physics of accretion in the first $\lesssim$700 million years of the Universe.

Author Contributions

N.P.R. initiated the project, compiled the list of $z > 5.00$ quasars, wrote most of the analysis code, developed the plotting scripts, and developed and wrote the initial and subsequent drafts of the manuscript.

N.J.G.C. supplied the critical near-infrared expertise and database for which the bulk of the project relies. N.J.G.C. also contributed directly to the writing of the manuscript.

Availability of Data and computer analysis codes

All materials, databases, data tables and code are fully available at: `https://github.com/d80b2t/VHzQ`

ACKNOWLEDGEMENTS

NPR acknowledges support from the STFC and the Ernest Rutherford Fellowship scheme.

We thank:

∘ Mike Read at the ROE WFAU for help with the WFCAM Science Archive (WSA) and the VISTA Science Archive (VSA).
∘ Tim Brooke at the IRSA Help Desk;
∘ Bernie Shiao at STScI for help with the Pan-STARRS1 DR1 CasJobs interface.
∘ Aaron Meisner and Eddie Schlafly for facilitating early access to the unWISE Catalog.
∘ Michael Cushing for supplying the Late Type stellar spectra and Beth Biller for useful discussion.

This paper heavily used TOPCAT (v4.4) (Taylor 2005, 2011). This research made use of `Astropy`, a community-developed core Python package for Astronomy (Astropy Collaboration et al. 2013; The Astropy Collaboration et al. 2018).

The VISTA Data Flow System pipeline processing and science archive were used for the WFCAM and VISTA near infrared data are described in Irwin et al (2004), Hambly et al (2008) and Cross et al. (2012).

The Pan-STARRS1 Surveys (PS1) and the PS1 public science archive have been made possible through contributions by the Institute for Astronomy, the University of Hawaii, the Pan-STARRS Project Office, the Max-Planck Society and its participating institutes, the Max Planck Institute for Astronomy, Heidelberg and the Max Planck Institute for Extraterrestrial Physics, Garching, The Johns Hopkins University, Durham University, the University of Edinburgh, the Queen's University Belfast, the Harvard-Smithsonian Center for Astrophysics, the Las Cumbres Observatory Global Telescope Network Incorporated, the National Central University of Taiwan, the Space Telescope Science Institute, the National Aeronautics and Space Administration under Grant No. NNX08AR22G issued through the Planetary Science Division of the NASA Science Mission Directorate, the National Science Foundation Grant No. AST-1238877, the University of Maryland, Eotvos Lorand University (ELTE), the Los Alamos National Laboratory, and the Gordon and Betty Moore Foundation.

This project used data obtained with the Dark Energy Camera (DECam) and the NOAO Data Lab, The Data Lab is operated by the National Optical Astronomy Observatory, the national center for ground-based nighttime astronomy in the United States operated by the Association of Universities for Research in Astronomy (AURA) under cooperative agreement with the National Science Foundation.

This publication makes use of data products from the Wide-field Infrared Survey Explorer, which is a joint project of the University of California, Los Angeles, and the Jet Propulsion Laboratory/California Institute of Technology, and NEOWISE, which is a project of the Jet Propulsion Laboratory/California Institute of Technology. WISE and NEOWISE are funded by the National Aeronautics and Space Administration.

CasJobs was originally developed by the Johns Hopkins University/ Sloan Digital Sky Survey (JHU/SDSS) team. With their permission, MAST used version 3.5.16 to construct CasJobs-based tools for GALEX, Kepler, the Hubble Source Catalog, and PanSTARRS.

This research has made use of the SVO Filter Profile Service (http://svo2.cab.inta-csic.es/theory/fps/) supported from the Spanish MINECO through grant AyA2014-55216 The SVO Filter Profile Service[10] de-

[10] Rodrigo, C., Solano, E., Bayo, A. http://ivoa.net/documents/Notes/SVOFPS/index.html

scribes the Spanish VO Filter Profile Service. The Filter Profile Service Access Protocol. Rodrigo, C., Solano, E. http://ivoa.net/documents/Notes/SVOFPSDAL/index.html

APPENDIX A: NEAR-INFRARED WFCAM SCIENCE ARCHIVE SQL QUERIES

Here we give the recipe and SQL that returned the near-infrared photometry for the VHzQs from the WFCAM Science Archive.

The data are on the WFCAM Science Archive: `wsa.roe.ac.uk`. Access the User Login form `wsa.roe.ac.uk/login.html` with these credentials::

- Username: `WSERV1000`
- password: `highzqso`
- community: `nonsurvey`

Then going to the `Free Form SQL Query` page the Database release `WSERV1000v20190507` can be accessed which contains all the data we use here.

We *nota bene* a few things. First, the quantity `aperJky3` and `aperJky3Err` are found in the `wserv1000MapRemeasAver` and `wserv1000MapRemeasurement`, so care has to be taken to return unique column names (otherwise e.g. astropy.io.fits will crash). As such, we alias `aver.aperJky3` to `aperJky3Aver` and likewise for the error quantity. Aliases will be necessary in some cases anyway, because some queries can be done sensibly on multiple instances of the same table. Other times, one may join tables on quantities such as `catalogueID` or `apertureID`, where you are meaning the same thing, but aliases are then necessary for SQLServer to correctly comprehend the query.

Second, the `RA` and `DEC` values returned by the WSA are in radians, if used directly. To return values in degrees, use a selection with an alias, e.g. `RA as RADeg` and `DEC as DECDeg`. Other relevant query examples can be found in the GitHub repository, under WSA_VSA/SAMPLE_SQL_QUERIES, or the SQLCookbook in the WSA or VSA.

Then the following SQL will return the values in Table **??**.

```
SELECT
qso.qsoName,  qso.ra as raJ2000, qso.dec as decJ2000,
aver.apertureID,  aver.aperJky3 as aperJky3Aver,
aver.aperJky3Err as aperJky3AverErr, aver.sumWeight,
aver.ppErrBits as ppErrBitsAver, m.mjdObs,
m.filterID, remeas.aperJky3,
remeas.aperJky3Err,
w.weight, remeas.ppErrBits,
m.project

FROM
finalQsoCatalogue as qso,
MapApertureIDshighzQsoMap as ma,
wserv1000MapRemeasAver as aver,
wserv1000MapRemeasurement as remeas,
MapProvenance as v,
wserv1000MapAverageWeights as w,
MapFrameStatus as mfs,
Multiframe as m

WHERE
qso.qsoID=ma.objectID and
ma.apertureID=aver.apertureID and
aver.apertureID=remeas.apertureID and
aver.catalogueID=v.combicatID and
v.avSetupID=1 and
v.catalogueID=remeas.catalogueID and
w.combicatID=v.combicatID and
w.catalogueID=v.catalogueID and
w.apertureID=aver.apertureID and
mfs.catalogueID=remeas.catalogueID and
m.multiframeID=mfs.multiframeID and
mfs.programmeID=10999 and
mfs.mapID=1
order by v.combicatID, m.mjdObs
```

APPENDIX B: NEAR-INFRARED VISTA SCIENCE ARCHIVE SQL QUERIES

In a very similar manner to the WSA, we give here the details on how to access the VISTA Science Archive (VSA)

At the VSA Login, enter with these credentials::

- Username: `VSERV1000`
- password: `highzqso`
- community: `proprietary`

Then head to the Freeform SQL Query page where the database release to use is `VSERV1000v20190508`. The queries are the same as those used in the WSA, see Appendix B, but the names of the tables starting with `wserv1000` should be replaced with `vserv1000`.

REFERENCES

Agarwal B., Smith B., Glover S., Natarajan P., Khochfar S., 2016, MNRAS, 459, 4209
Alexander T., Natarajan P., 2014, Science, 345, 1330
Assef R. J., et al., 2012, arXiv:1209.6055v1,
Assef R. J., Stern D., Noirot G., Jun H. D., Cutri R. M., Eisenhardt P. R. M., 2018, ApJS, 234, 23
Astropy Collaboration et al., 2013, Astron. & Astrophys., 558, A33
Bañados E., et al., 2014, AJ, 148, 14
Bañados E., et al., 2016, ApJS, 227, 11
Bañados E., et al., 2018, Nat, 553, 473
Becker R. H., White R. L., Helfand D. J., 1995, ApJ, 450, 559
Becker G. D., Bolton J. S., Lidz A., 2015, PASA, 32, 45
Becker G., D'Aloisio A., Davies F. B., Hennawi J. F., Simcoe R. A., 2019, in BAAS. p. 440 (arXiv:1903.05199)
Bilicki R., et al., 2016, ApJS, 225, 5
Blain A., et al., 2013, preprint, (arXiv:1310.2301)
Bosman S. E. I., et al., 2017, MNRAS, 470, 1919
Brown M. J. I., Jarrett T. H., Cluver M. E., 2014, PASA, 31, 49
Calura F., Gilli R., Vignali C., Pozzi F., Pipino A., Matteucci F., 2014, MNRAS, 438, 2765
Carilli C. L., et al., 2007, ApJ Lett., 666, L9
Carilli C. L., et al., 2010, ApJ, 714, 834
Carnall A. C., et al., 2015, MNRAS, 451, L16
Casali M., et al., 2007, Astron. & Astrophys., 467, 777
Chen S.-F. S., et al., 2017, ApJ, 850, 188
Civano F., et al., 2011, ApJ, 741, 91
Cool R. J., et al., 2006, AJ, 132, 823
Cross N. J. G., et al., 2012, Astron. & Astrophys., 548, A119
Cross N., Hambly N., Collins R., Sutorius E., Read M., Blake R., 2013, in Adamson A., Davies J., Robson I., eds, Astrophysics and Space Science Proceedings Vol. 37, Thirty Years of Astronomical Discovery with UKIRT. p. 193, doi:10.1007/978-94-007-7432-2˙17
Cushing M. C., et al., 2006, ApJ, 648, 614
Cutri R. M. o., 2013, Technical report, Explanatory Supplement to the AllWISE Data Release Products
Dalton G. B., et al., 2006, in Society of Photo-Optical Instrumentation Engineers (SPIE) Conference Series. p. 62690X, doi:10.1117/12.670018
De Rosa G., Decarli R., Walter F., Fan X., Jiang L., Kurk J., Pasquali A., Rix H. W., 2011, ApJ, 739, 56
Dey A., et al., 2018, preprint, (arXiv:1804.08657)
Dye S., et al., 2018, MNRAS, 473, 5113
Edge A., Sutherland W., Kuijken K., Driver S., McMahon R., Eales S., Emerson J. P., 2013, The Messenger, 154, 32
Emerson J. P., et al., 2004, in P. J. Quinn & A. Bridger ed., Society of Photo-Optical Instrumentation Engineers (SPIE) Conference Series Vol. 5493, Society of Photo-Optical Instrumentation Engineers (SPIE) Conference Series. pp 401–410, doi:10.1117/12.551582
Emerson J., McPherson A., Sutherland W., 2006, The Messenger, 126, 41
Fan X., et al., 2000, AJ, 119, 1
Fan X., et al., 2001a, AJ, 121, 54
Fan X., et al., 2001b, AJ, 122, 2833
Fan X., et al., 2003, AJ, 125, 1649
Fan X., et al., 2004, AJ, 128, 515
Fan X., Carilli C. L., Keating B., 2006a, ARA&A, 44, 415
Fan X., et al., 2006b, AJ, 132, 117
Fan X., et al., 2018, preprint, (arXiv:1810.11924)
Fan X., et al., 2019a, in BAAS. p. 121 (arXiv:1903.04078)
Fan X., et al., 2019b, ApJ, 870, L11
Fukugita M., Ichikawa T., Gunn J. E., Doi M., Shimasaku K., Schneider D. P., 1996, AJ, 111, 1748
Gezari S., et al., 2017, ApJ, 835, 144
Glikman E. o., 2018, ApJ, 861, 37
Glikman E., et al., 2018, arXiv e-prints, p. arXiv:1807.05434
Goto T., 2006, MNRAS, 371, 769
Graham M. J., et al., 2019, arXiv e-prints, p. arXiv:1905.02262
Haardt F., Gorini V., Moschella U., Treves A., Colpi M., eds, 2016, Astrophysical Black Holes Lecture Notes in Physics, Berlin Springer Verlag Vol. 905, doi:10.1007/978-3-319-19416-5.
Hambly N. C., et al., 2008, MNRAS, 384, 637
Hickox R. C., Myers A. D., Greene J. E., Hainline K. N., Zakamska N. L., DiPompeo M. A., 2017, ApJ, 849, 53
Hill A. R., Gallagher S. C., Deo R. P., Peeters E., Richards G. T., 2014, MNRAS, 438, 2317
Ikeda H., et al., 2012, ApJ
Ikeda H., Nagao T., Matsuoka K., Kawakatu N., Kajisawa M., Akiyama M., Miyaji T., Morokuma T., 2017, ApJ, 846, 57
Jannuzi B. T., Dey A., 1999, in Weymann R., et al., eds, ASP Conf. Ser. 191: Photometric Redshifts and the Detection of High Redshift Galaxies. p. 111
Jiang L., et al., 2006, AJ, 132, 2127
Jiang L., et al., 2008, AJ, 135, 1057
Jiang L., et al., 2009, AJ, 138, 305
Jiang L., et al., 2010, Nat, 464, 380
Jiang L., McGreer I. D., Fan X., Bian F., Cai Z., Clément B., Wang R., Fan Z., 2015, AJ, 149, 188
Jiang L., et al., 2016, ApJ, 833, 222
Kaiser N., et al., 2002, in Tyson J. A., Wolff S., eds, Society of Photo-Optical Instrumentation Engineers (SPIE) Conference Series Vol. 4836, Survey and Other Telescope Technologies and Discoveries. pp 154–164, doi:10.1117/12.457365
Kaiser N., et al., 2010, in Society of Photo-Optical Instrumentation Engineers (SPIE). p. 0, doi:10.1117/12.859188
Kashikawa N., et al., 2015, ApJ, 798, 28
Kim Y., et al., 2015, ApJ Lett., 813, L35
Kim Y., et al., 2018, preprint, (arXiv:1811.08606)
Koptelova E., Hwang C.-Y., Yu P.-C., Chen W.-P., Guo J.-K., 2017, Scientific Reports, 7, 41617
Krawczyk C. M., Richards G. T., Mehta S. S., Vogeley M. S., Gallagher S. C., Leighly K. M., Ross N. P., Schneider D. P., 2013, ApJS, 206, 4
Kurk J. D., et al., 2007, ApJ, 669, 32
Kurk J. D., Walter F., Fan X., Jiang L., Jester S., Rix H.-W., Riechers D. A., 2009, ApJ, 702, 833
LaMassa S. M., et al., 2015, ApJ, 800, 144
LaMassa S. M., et al., 2017, ApJ, 847, 100
LaMassa S. M., et al., 2019, ApJ, 876, 50
Lacy M., et al., 2004, ApJS, 154, 166
Lang D., 2014, AJ, 147, 108
Latif M. A., Volonteri M., Wise J. H., 2018, arXiv:1801.07685v1,
Lawrence A., et al., 2007, MNRAS, 379, 1599

Le Fèvre O., et al., 2003, in Iye M., Moorwood A. F. M., eds, Proc. SPIEVol. 4841, Instrument Design and Performance for Optical/Infrared Ground-based Telescopes. pp 1670–1681, doi:10.1117/12.460959
Leipski C., et al., 2014, ApJ, 785, 154
Lupi A., Haardt F., Dotti M., Fiacconi D., Mayer L., Madau P., 2016, MNRAS, 456, 2993
MacLeod C. L., Ross N. P., et al., 2016, MNRAS, 457, 389
MacLeod C. L., et al., 2019, ApJ, 874, 8
Madau P., Haardt F., Dotti M., 2014, ApJ Lett., 784, L38
Mahabal A., Stern D., Bogosavljević M., Djorgovski S. G., Thompson D., 2005, ApJ Lett., 634, L9
Mainzer A., et al., 2011, ApJ, 731, 53
Mainzer A., et al., 2014, ApJ, 792, 30
Matsuoka Y., et al., 2016, ApJ, 828, 26
Matsuoka Y., et al., 2018a, PASJ, 70, S35
Matsuoka Y., et al., 2018b, ApJS, 237, 5
Mazzucchelli C., et al., 2017, ApJ, 849, 91
McGreer I. D., Becker R. H., Helfand D. J., White R. L., 2006, ApJ, 652, 157
McGreer I. D., et al., 2013, ApJ, 768, 105
McGreer I. D., Fan X., Jiang L., Cai Z., 2018, AJ, 155, 131
Meisner A. M., Lang D., Schlegel D. J., 2017, AJ, 153, 38
Meisner A. M., Lang D., Schlegel D. J., 2018a, Research Notes of the American Astronomical Society, 2, 1
Meisner A. M., Lang D. A., Schlegel D. J., 2018b, Research Notes of the American Astronomical Society, 2, 202
Miyazaki S., et al., 2018, PASJ, 70, S1
Morganson E., et al., 2012, AJ, 143, 142
Mortlock D., 2016, in Mesinger A., ed., Astrophysics and Space Science Library Vol. 423, Understanding the Epoch of Cosmic Reionization: Challenges and Progress. p. 187 (arXiv:1511.01107), doi:10.1007/978-3-319-21957-8˙7
Mortlock D. J., et al., 2009, Astron. & Astrophys., 505, 97
Mortlock D. J., et al., 2011, Nat, 474, 616
Oke J. B., Gunn J. E., 1983, ApJ, 266, 713
Pezzulli E., Valiante R., Schneider R., 2016, MNRAS, 458, 3047
Pezzulli E., Volonteri M., Schneider R., Valiante R., 2017, MNRAS, 471, 589
Planck Collaboration 2016, Astron. & Astrophys., 594, A13
Reed S. L., et al., 2015, MNRAS, 454, 3952
Reed S. L., et al., 2017, MNRAS, 468, 4702
Rees M. J., 1984, ARA&A, 22, 471
Regan J. A., et al., 2019, MNRAS, 486, 3892
Richards G. T., et al., 2006, ApJS, 166, 470
Ross N. P., et al., 2013, ApJ, 773, 14
Ross N. P., et al., 2015, MNRAS, 453, 3932
Ross N. P., et al., 2018, MNRAS, 480, 4468
Ross N., Assef R. J., Kirkpatrick J. D., Graham M. J., 2019, in BAAS. p. 321 (arXiv:1904.06160)
Ruan J. J., et al., 2016, ApJ, 826, 188
Runco J. N., et al., 2016, ApJ, 821, 33
Runnoe J. C., et al., 2016, MNRAS, 455, 1691
Sawicki M., 2002, AJ, 124, 3050
Schlafly E. F., Meisner A. M., Green G. M., 2019, ApJS, 240, 30
Secrest N. J., et al., 2015, ApJS, 221, 12
Shanks T., et al., 2015, MNRAS, 451, 4238
Simcoe R. A., Sullivan P. W., Cooksey K. L., Kao M. M., Matejek M. S., Burgasser A. J., 2012, Nat, 492, 79
Stern D., et al., 2005, ApJ, 631, 163
Stern D., et al., 2007, ApJ, 663, 677
Stern D., et al., 2012, ApJ, 753, 30
Stern D., et al., 2018, ApJ, submitted
Stoughton C., et al., 2002, AJ, 123, 485
Takeo E., Inayoshi K., Ohsuga K., Takahashi H. R., Mineshige S., 2018, MNRAS, 476, 673
Tang J.-J., et al., 2017, MNRAS, 466, 4568
Taylor M. B., 2005, in Shopbell P., Britton M., Ebert R., eds, Astronomical Society of the Pacific Conference Series Vol. 347, Astronomical Data Analysis Software and Systems XIV. p. 29
Taylor M., 2011, TOPCAT: Tool for OPerations on Catalogues And Tables, Astrophysics Source Code Library (ascl:1101.010)
The Astropy Collaboration et al., 2018, preprint, (arXiv:1801.02634v2)
Tielens A. G. G. M., 2008, ARA&A, 46, 289
Timlin J. D., Ross N. P., et al., 2016, ApJS, 225, 1
Väisänen P., Tollestrup E. V., Willner S. P., Cohen M., 2000, ApJ, 540, 593
Valiante R., Schneider R., Graziani L., Zappacosta L., 2018, MNRAS, 474, 3825
Vanden Berk D. E., et al., 2001, AJ, 122, 549
Venemans B. P., McMahon R. G., Warren S. J., Gonzalez-Solares E. A., Hewett P. C., Mortlock D. J., Dye S., Sharp R. G., 2007, MNRAS, 376, L76
Venemans B. P., et al., 2012, ApJ Lett., 751, L25
Venemans B. P., et al., 2013, ApJ, 779, 24
Venemans B. P., et al., 2015a, MNRAS, 453, 2259
Venemans B. P., et al., 2015b, ApJ Lett., 801, L11
Venemans B. P., Walter F., Zschaechner L., Decarli R., De Rosa G., Findlay J. R., McMahon R. G., Sutherland W. J., 2016, ApJ, 816, 37
Volonteri M., 2010, A&ARv, 18, 279
Volonteri M., Silk J., Dubus G., 2015, ApJ, 804, 148
Wang R., et al., 2008, ApJ, 687, 848
Wang R., et al., 2011, ApJ Lett., 739, L34
Wang F., et al., 2016, ApJ, 819, 24
Wang F., et al., 2017, ApJ, 839, 27
Wang F., et al., 2018b, arXiv:1810.11926v1,
Wang F., et al., 2018a, arXiv:1810.11925v1,
Wang L., et al., 2019, in BAAS. p. 399 (arXiv:1903.06027)
Willott C. J., et al., 2007, AJ, 134, 2435
Willott C. J., et al., 2009, AJ, 137, 3541
Willott C. J., et al., 2010, AJ, 139, 906
Willott C. J., Omont A., Bergeron J., 2013, ApJ, 770, 13
Willott C. J., Bergeron J., Omont A., 2015, ApJ, 801, 123
Wise J. H., Regan J. A., O'Shea B. W., Norman M. L., Downes T. P., Xu H., 2019, arXiv:1901.07563v1,
Wright E. L., Eisenhardt P. E., Fazio G. G., 1994, ArXiv Astrophysics e-prints,
Wright E. L., et al., 2010, AJ, 140, 1868
Wu X.-B., et al., 2015, Nat, 518, 512
Wyithe J. S. B., Loeb A., 2003, ApJ, 586, 693
Yan L., et al., 2007, ApJ, 658, 778
Yang J., et al., 2017, AJ, 153, 184
Yang J., et al., 2018b, arXiv:1811.11915v1,
Yang J., et al., 2018a, arXiv:1810.11927v1,
Yang Q., et al., 2018c, ApJ, 862, 109
Zeimann G. R., White R. L., Becker R. H., Hodge J. A., Stanford S. A., Richards G. T., 2011, ApJ, 736, 57